Vol. **114** (2008) *ACTA PHYSICA POLONICA A* Supplement

Proceedings of the Professor Stefan Mróz Symposium

Surface Chemistry of Zirconia Nanopowders Doped with Pr_2O_3: an XPS Study

Y. Suchorski[a,*], R. Wrobel[b,†], S. Becker[b], A. Opalińska[c], U. Narkiewicz[d], M. Podsiadly[d] and H. Weiss[b]

[a]Institute of Materials Chemistry, Vienna University of Technology
Veterinärplatz 1, A-1210 Vienna, Austria
[b]Chemisches Institut, Otto-von-Guericke-Universität Magdeburg
Universitätsplatz 2, D-39106 Magdeburg, Germany
[c]Institute of High Pressure Physics, Polish Academy of Sciences
Sokołowska 29, 01-142 Warsaw, Poland
[d]Institute of Chemical and Environment Engineering
Szczecin University of Technology
Pułaskiego 10, 70-322 Szczecin, Poland

Zirconia nanopowders of tetragonal crystallographic structure doped with Pr_2O_3 were prepared by the microwave-assisted hydrothermal synthesis and coprecipitation method. The surface compositions were studied by X-ray photoelectron spectroscopy. The nanopowder particles appear to be inhomogeneous in their structure: for the surface region an enrichment with praseodymium is detected by X-ray photoelectron spectroscopy measurements. This allows the assumption of a core-shell-like structure of single nanopowders particles. The X-ray photoelectron spectroscopy studies confirm also Zr^{4+} and Pr^{3+} as main oxidation states of zirconium and praseodymium in the studied compounds.

PACS numbers: 79.60.–i, 61.46.–w, 61.46.Hk

1. Introduction

Zirconia related materials have attracted in the last decades increasing attention of both researchers and manufacturers because of the wide variety of applications which spread from the jewellery industry to substrates for the growth of superconductors [1] to the nanopowders used in catalysis [2–4]. Due to the

*corresponding author; e-mail: yuri.suchorski@imc.tuwien.ac.at
†On leave from Technical University of Szczecin, Szczecin, Poland.

high thermal and chemical stability accompanied by significant mechanical-stress resistivity zirconia is applied in the ceramic industry [5] and for thermal barrier coatings (TBCs) [6]. The fact that zirconia is very stable over the pH range of 1–14 [7] allows a sample packing application in high-performance liquid chromatography (HPLC). Biomedical applications of zirconia are reported as well, as for example for implants or dental ceramics [8].

Unfortunately, the phase transition of zirconia from the monoclinic to the tetragonal system (at 1400 K) restricts its high-temperature use. Yttria, calcia, ceria or oxides of rare-earth metals (e.g. Er, La, Pr) allows to improve the thermal stability of zirconia [9–14]. With these stabilizers the zirconia structure becomes a cubic solid solution which shows no phase transformation up to the melting point [15]. Being a good ceramic ion conductor, stabilized zirconia is used in oxygen sensors and in solid oxide fuel cells (SOFCs) [16]. A further interesting application of zirconia is related to its luminescent properties [17, 18], where the dependence of the luminescence characteristics on the number of oxygen vacancies makes it a promising material for an optical oxygen pressure sensor [19].

In heterogeneous catalysis zirconia-containing mixed oxides are used as a support for catalytically active noble metal particles or as a catalyst itself e.g. for selective NO_x reduction with hydrocarbons or CO [20–23]. Addition of ZrO_2 to ceria based catalysts enhances the thermal stability and the oxygen storage capacity of pure ceria, resulting in better performance in diesel soot combustion [24] due to more reactive oxygen ions, similarly as was observed in three way catalysts [25].

Progress in the synthesis of zirconia materials with a well developed surface area (nanopowders with controlled size, porosity and chemical composition) may significantly improve the performance of the commercially used zirconia-containing catalysts. It was shown, e.g., that the catalytic activity of Au nanoparticles (4–5 nm) in Au/ZrO_2 can be enhanced remarkably when the particle size of the zirconia "support" decreases from 100 to 5 nm [26]. Zirconia nanopowders may also be applied directly as catalysts for the decomposition of N_2O [27], for selective reduction of NO with methane [28] or for esterification of acrylic acid with but-1-ene [29].

Most of the above-mentioned applications of zirconia-based materials, especially of nanopowders, are related to their surface properties and to the dopant effects. Thus there is an evident need for a surface characterization of variously doped zirconia nanopowders prepared using different methods. A direct insight into the chemical composition and chemical state of the surface species can be gained by X-ray photoelectron spectroscopy (XPS). We present in this study a detailed XPS study of zirconia nanopowders doped with Pr_2O_3.

2. Experimental

The Pr_2O_3 doped zirconia nanopowders were obtained by two different methods: coprecipitation from aqueous solution of $ZrOCl_2$ and $Pr(NO_3)_3$ using 1 M

solution of NaOH as precipitating agent, and the microwave-assisted hydrothermal method.

During the precipitation at increasing pH values, samples of the solution were taken for different values of pH to measure the concentrations of Zr and Pr using inductively coupled plasma atomic emission spectroscopy (ICP-AES, Yvon--Jobin, France). The precipitation was considered as completed at pH = 10, and was followed by calcination at 773 K in air for 3 h.

The alternative procedure of nanopowder preparation was the microwave--assisted hydrothermal method. The same solutions as for the precipitation were poured at 543 K and under the pressure of 5.5 MPa in a PTFE reaction vessel of the microwave reactor (ERTEC, Poland), operating at 2.45 GHz and at power density adjusted to 4 W/ml.

The resulting chemical composition of the prepared samples was determined using ICP-AES, and the phase composition of the samples as well as their mean crystallite size was obtained by X-ray diffraction (XRD) analysis (Philips X-Pert powder diffractometer with Co K_{α_1} radiation). The specific surface area measurements were conducted by means of the multipoint Brunauer–Emmett–Teller (BET) method (Micromeritics Instruments, USA), using nitrogen as adsorbate.

The surface properties were studied in a commercial multipurpose UHV surface analysis system with XPS, low energy electron diffraction (LEED), scanning tunneling microscopy (STM), ultraviolet photoelectron spectroscopy (UPS), and the Auger electron spectroscopy (AES) (SPECS, Germany) operating at base pressures around 10^{-10} mbar. The XP-spectra were recorded with a 150 mm hemispherical energy analyzer (Phoibos-150, SPECS) which allows a simultaneous photoelectron detection on 9 channels, and permits thus fast data acquisition times (0.5 s per data point) with a satisfactory signal-to-noise ratio. In the present study, a standard high-intensity Al/Mg twin anode X-ray source (XR-50, SPECS) has been used, mainly in a "stop-and-go" mode in order to reduce sample irradiation (Mg K_α, excitation energy 1253.6 eV, 150 W) just to the period of data acquisition only to avoid the X-ray induced photoreduction of surface regions [30]. A possible vacuum-induced reduction of the samples was minimized by fast sample transfer (less than 5 min between the start of the evacuation of the load lock and the first XP-spectrum at a pressure better than 5×10^{-10} mbar [31]). High--resolution spectra (pass energy 10 eV, step size 0.1–0.2 eV) of the Pr 3*d*, Zr 3*d*, and O 1*s* regions as well as the survey spectra were measured with the largest possible aperture in order to obtain maximum signal intensity. The work function of the analyzer was calibrated using the binding energy (BE) value of 84.0 eV for the Au $4f_{7/2}$ signal from a clean gold foil. The deconvolution of the XP-peaks as well as the whole evaluation of the spectra was performed using the CasaXPS software package [32].

3. Results and discussion

During precipitation the concentration of zirconium and praseodymium in an aqueous solution of $ZrOCl_2$ and $Pr(NO_3)_3$ changes, since zirconium hydroxide precipitates at remarkably lower pH-values than praseodymium hydroxide. As one can see in Fig. 1, only about 25% of the zirconium ions are still present in the solution at pH = 4 (i.e. $\approx$ 75% of Zr is precipitated as hydroxide) and, simultaneously, less than a quarter of praseodymium is precipitated at this pH value.

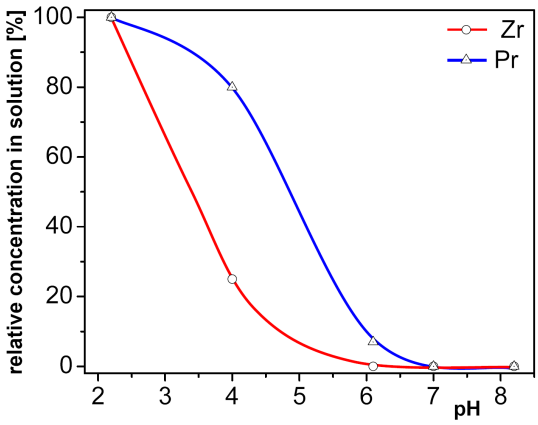

Fig. 1. Relative concentrations of zirconium and praseodymium ions in the solution during the precipitation process.

Such differences in solubility of Pr and Zr at different pH-values may lead to inhomogeneities in the structure of the resulting particles: each of them might be composed of a core containing mainly zirconium hydroxide and of a shell in which praseodymium is prevailing. We note that for pH-values between 6 and 7 almost pure Pr is precipitated leading thus presumably to a praseodymium hydroxide shell over on top of the grains.

It is interesting to compare the properties of the zirconia samples with a similar quantity of the dopant but obtained by different methods (coprecipitation via hydrothermal). This was done for samples with 4.6 and 7.4 wt.% of Pr_2O_3, respectively. The BET measurements reveal that the samples obtained by the hydrothermal method appear to be more porous: their specific surface area ranged up to 145 m^2/g and was significantly higher than those of the samples prepared by coprecipitation, whose surface area reached 33 m^2/g only.

The XRD analysis for both samples shows that the powder particles are of nanometric size (the mean crystallite size of zirconia particles prepared by the hydrothermal method and by coprecipitation was 7 nm and 9 nm, respectively). The slightly smaller size of the particles obtained with hydrothermal method do not justify the over four times higher surface area. This apparent discrepancy

indicates that in case of the coprecipitation method the crystallites tend to form clusters. Formation of clusters does not affect the XRD measurements (crystallites size) significantly but strongly affects the BET results due to the lower exposed surface area necessary for the adsorption of the nitrogen.

The tetragonal form of zirconia with some traces of the monoclinic phase was detected by XRD in both types of samples. However, at room temperature the known stable form of pure zirconia of "non-nanocrystalline" size is monoclinic. The different stable crystallographic system of doped samples seems to be due to the stabilizing effect of praseodymium oxide and the nanometric size of the particles. Several authors confirm that the tetragonal phase can be observed at room temperature for the zirconia nanoparticles with a critical size of about 30 nm [33].

To investigate the surface properties of the zirconia nanopowders doped with praseodymium oxide, and to evaluate the oxidation state of Zr and Pr in the compounds, XPS studies were carried out on two different samples prepared by the hydrothermal method and containing 5 and 18 wt.% of Pr_2O_3, respectively. Identification of the oxidation states of metals in their oxide compounds via XPS is a challenging task in the majority of cases, especially for powder samples. However, in the present case of praseodymium the characteristic shape of the $3d_{3/2}$ and $3d_{5/2}$ peaks allows an unambiguous identification even without the exact knowledge of the peak positions. The characteristic shoulders s and s' on the low energy sides of both Pr $3d$ peaks do not appear in the Pr $3d$ spectra for the metallic praseodymium but, in turn, form a clearly visible satellite structure with adjacent minima in the case of PrO_2 [34–37]. These minima remain invisible in the Pr_2O_3 case, as it is demonstrated in Ref. [34] and clearly seen in Fig. 2a. Thus in our compounds the praseodymium is present mostly in the Pr^{3+} state.

This unambiguous identification allows us to assign the position of the Pr $3d_{5/2}$ peak to the literature BE value of 933.6 eV for Pr_2O_3 [34, 35]. This permits a possibility to consider properly the charging effects in the studied samples. The correspondingly calibrated energy scale assigns then the O $1s$ peak with the BE of 529.8 eV to oxygen from ZrO_2 whereas a rather minor contribution located at 529.1 eV can be attributed to Pr_2O_3 and a hydroxide formation causes a shoulder on the high-energy side at 532 eV (Fig. 2b). The above value of 529.8 eV is in nice agreement with the known literature data for ZrO_2 [38] and the value of 529.1 eV matches exactly the known O $1s$ peak position for the pure Pr_2O_3 [36].

Figure 3c shows the corresponding $3d_{3/2}$ and $3d_{5/2}$ peaks for Zr which are found at 181.9 eV and 184.3 eV, respectively, also in good agreement with the literature data for ZrO_2 [36, 39]. Although the above positions of the Zr $3d_{3/2}$ and $3d_{5/2}$ peaks provide a strong suggestion that Zr^{4+} is the main oxidation state of Zr, the FWHMs have to be taken into account under the aspect of a possible suboxide contribution. However the, for powder samples, relatively narrow FWHMs of 1.66 eV and 1.75 eV for the Zr $3d_{3/2}$ and $3d_{5/2}$ lines, correspondingly, support strongly the suggestion of the dominance of Zr^{4+} in the studied compounds.

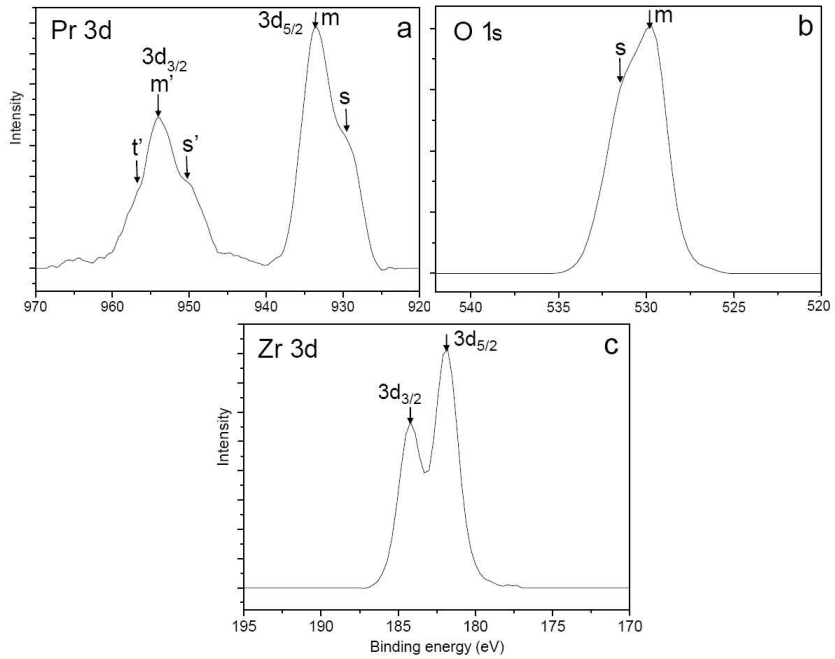

Fig. 2. High resolution XP-spectra of the "18%" sample: (a) Pr 3d region, note the shoulders s' and s in the Pr $3d_{3/2}$ and in the Pr $3d_{5/2}$ peaks correspondingly, as well as the feature t' in the Pr $3d_{3/2}$ peak (the indexing and the assignment of the features m, m', s, s', and t' correspond to those of Ref. [28]); (b) O 1s peak, note the shoulder s on the high energy side (at 532 eV); (c) Zr 3d region, the FWHMs of the Zr $3d_{3/2}$ and Zr $3d_{5/2}$ peaks amounts 1.66 and 1.75 eV, correspondingly.

Additionally, the energy difference between the O 1s and metal 3d lines can be used as a measure for an (effective) "average oxidation state" of a metal in an oxide compound. This method is often used when the deconvolution appears to be difficult, e.g. when the powder materials are studied, where the differential charging might deform the peaks leading to the appearance of "apparent" oxidation states. Recent applications to the vanadium-based oxide catalysts demonstrated the usefulness of such a criterion [31, 40]. In the present case, the energy difference between the Zr $3d_{5/2}$ line and the main O 1s peak amounts to 347.9 eV in a perfect agreement with the known literature data (347.9 eV is reported in Ref. [36] for pure ZrO_2, similar values are obtained elsewhere [41, 42]). Since this criterion is independent of the charging effects as well as of the calibration of the energy scale, and due to a significant chemical shift of Zr 3d region of 4.23 eV in respect of the pure Zr-metal [42], one can conclude with a sufficient reliability that no reduction of ZrO_2 is observed and also none of possible UHV-induced [31] or photoreduction (caused by X-rays [30]) effects take place under the present conditions.

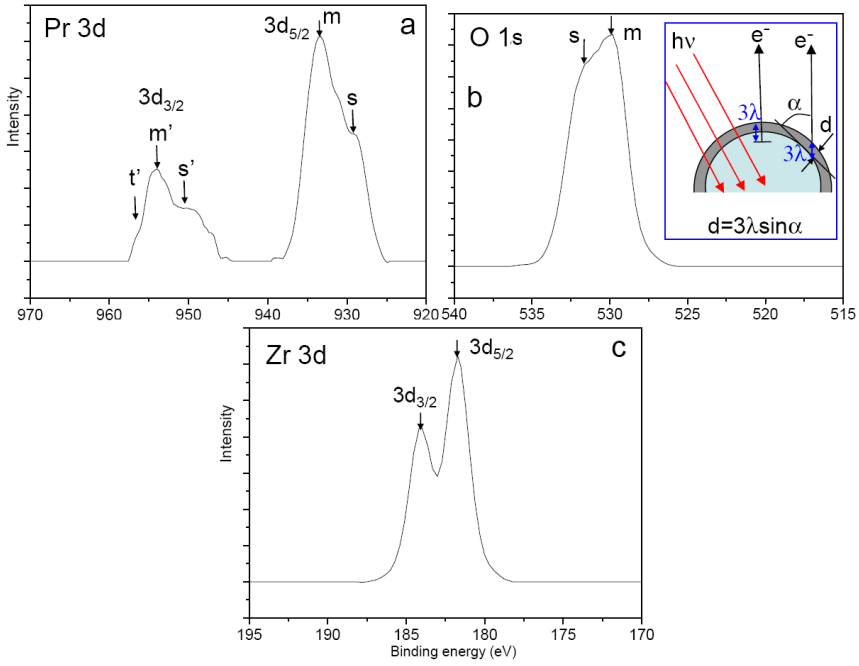

Fig. 3. An XPS analysis of the "5%" sample: (a) Pr 3*d* region, similarly as in Fig. 1a, the s' and s shoulders, typical of Pr^{3+} and the t' feature are well visible; (b) O 1*s* peak, the inset illustrates the basic mechanism enhancing the surface sensitivity for bent surface of powder particles (see text); (c) Zr 3*d* region, the Zr $3d_{3/2}$ and Zr $3d_{5/2}$ peak positions (184.2 and 181.8 eV, correspondingly) provide an evidence for the dominance of the Zr^{4+} in the sample.

A quantitative comparison of the Pr and Zr 3*d* contributions demonstrates that the Pr_2O_3 concentration in the sample regions from which the information carriers originate is by a factor of 3.1 higher than in the initial sample composition. For the used energy interval the information depth (ID) ranges in the present case between 0.6 and 1.8 nm [43], however, because powder particles are analyzed here, the contribution of the topmost surface layers is even higher than it would be in the flat surface case. The reason for this lies in the variation of the take-off angle for the bended surface of a powder particle. The sampling depth and thereby the degree of surface sensitivity of XPS varies with the take-off angle as $d = 3\lambda \sin\alpha$, where d is the sampling depth and λ is the effective attenuation length (EAL), α is the take-off angle. The value 3λ results from the Lambert–Beer law in the assumption that 95% of the signal intensity is obtained normal to the surface from this depth [44, 45]. For the relation between the sampling depth, EAL, inelastic mean free path (IMFP) and for the role of elastic-scattering of XP-electrons that causes differences between the EAL and IMFP, see review [45].

A surface, bent on a scale much bigger than the EAL, produces deviations in the ID since the electron exit angle at a given surface point will generally be different from that defined with respect to the macroscopic sample plane held parallel to the analyzer acceptance plane. Of course, the exact values of such deviations are strongly related to the particular shape of the surfaces, but generally, for a powder particle a disproportionally high contribution of the topmost surface layer in the XP-signal is expected since a significant part of the XP-electrons originate from the sloping part of the particle surface. The inset in Fig. 3b illustrates these considerations. Therefore we conclude from the present data that segregation of the Pr_2O_3 additive in the surface regions takes place.

Figure 3a–c shows the high-resolution XP-spectra measured for the "5%" sample. Following the same procedure as described above for the sample containing 18% of Pr_2O_3, the binding energies of 954.1 and 933.6 eV were assigned to the Pr $3d_{3/2}$ and Pr $3d_{5/2}$ peaks, respectively. This assignment yields the value of 529.9 eV for the O $1s$ peak (oxygen from ZrO_2) and of 184.2 and 181.8 eV for the Zr $3d_{3/2}$ and Zr $3d_{5/2}$ peaks, correspondingly. A shoulder on the high energy side from hydroxide appears at 531.8 eV and the oxygen contribution from Pr_2O_3 is hardly detectable because of its small concentration. Similarly, as in the case of another sample a surface segregation of Pr_2O_3 may be stated, whereas the concentration of the Pr-additive in studied regions is by factor 2.2 higher than that in the initial compound.

4. Conclusions

The comparative measurements for zirconia nanopowders doped with Pr_2O_3 as prepared by the microwave-assisted hydrothermal synthesis and by standard coprecipitation show that the samples prepared using the first way exhibit a smaller crystallite size and a larger surface area than those obtained by the second method. The stabilizing effect of the praseodymium oxide and the nanometric size causes that the stable system has a tetragonal structure at room temperature for both kinds of samples. The composition of the nanoparticles prepared by both methods appears to be inhomogeneous: for the surface region an enrichment with praseodymium oxide is detected which was attributed to the Pr and Zr concentration dependence during the precipitation. This allows an assumption of a core-shell-like structure of single nanopowder particles. The XPS studies confirm also Zr^{4+} and Pr^{3+} as main oxidation states of zirconium and praseodymium in the studied compounds.

References

[1] D.M. Hwang, Q.Y. Ying, H.S. Kwok, *Appl. Phys. Lett.* **58**, 2429 (1991).

[2] S. Furuta, H. Matsuhashi, K. Arata, *Biomass Bioenerg.* **30**, 870 (2006).

[3] J.R. Sohn, S.H. Lee, J.S. Lim, *Catal. Today* **116**, 143 (2006).

[4] J. Zhu, J.G. van Ommen, H.J.M. Bouwmeester, L. Lefferts, *J. Catal.* **233**, 434 (2005).

[5] http://www.heqingceramics.com.

[6] J. Moon, H. Choi, H. Kim, C. Lee, *Surf. Coat. Tech.* **155**, 1 (2002).

[7] J.A. Blackwell, P.W. Carr, *J. Chromatogr.* **549**, 59 (1991).

[8] J. Chevalier, *Biomaterials* **27**, 535 (2006).

[9] R.I. Merino, J.I. Pena, M.A. Laguna-Bercero, A. Larrea, V.M. Orera, *J. Eur. Ceram. Soc.* **24**, 1349 (2004).

[10] W.B. Gong, C.K. Sha, D.Q. Sun, W.Q. Wang, *Surf. Coat. Tech.* **201**, 3109 (2006).

[11] S.T. Aruna, K.S. Rajam, *Scr. Mater.* **48**, 507 (2003).

[12] J.R. De la Rosa, A. Hernandez, F. Rojas, J.J. Ledezma, *Colloid. Surface A* **315**, 147 (2008).

[13] B. Savoini, J.E. Munoz-Santiuste, R. Gonzalez, G.K. Cruz, C. Bonardi, R.A. Carvalho, *J. Alloy. Comp.* **323-324**, 748 (2001).

[14] M. Kunz, H. Kretschmann, W. Assmus, C. Klingshirn, *J. Lumin.* **37**, 123 (1987).

[15] http://www.stanfordmaterials.com/zro2.html.

[16] C. Brahim, A. Ringuede, M. Cassir, M. Putkonen, L. Niinisto, *Appl. Surf. Sci.* **253**, 3962 (2007).

[17] H. Yugami, A. Koike, M. Ishigame, *Phys. Rev. B* **44**, 9214 (1991).

[18] K. Smits, L. Grigorjeva, W. Łojkowski, J.D. Fidelus, *Phys. Status Solidi C* **4**, 770 (2007).

[19] J.D. Fidelus, W. Lojkowski, D. Millers, L. Grigorjeva, K. Smits, R.R. Piticescu, *Solid State Phenom.* **128**, 141 (2007).

[20] L. Zenboury, B. Azambre, J.V. Weber, *Catal. Today*, 2008, in press.

[21] P. Fornasiero, G. Ranga Rao, J. Kaspar, F. L'Erario, M. Graziani, *J. Catal.* **175**, 269 (1998).

[22] M. Adamowska, S. Muller, P. Da Costa, A. Krzton, P. Burg, *Appl. Catal. B-Environ.* **74**, 278 (2007).

[23] C. Thomas, O. Gorce, C. Fontaine, J.M. Krafft, F. Villain, G. Djéga-Maiadassoua, *Appl. Catal. B-Environ.* **63**, 201 (2006).

[24] E. Aneggi, C. de Leitenburg, G. Dolcetti, A. Trovarelli, *Catal. Today* **114**, 40 (2006).

[25] H.S. Gandhi, G.W. Graham, R.W. McCabe, *J. Catal.* **216**, 433 (2003).

[26] Xin Zhang, Hai Wang, Bo-Qing Xu, *J. Phys. Chem. B* **109**, 9678 (2005).

[27] P. Granger, P. Esteves, S. Kieger, L. Navascues, G. Leclercq, *Appl. Catal. B-Environ.* **62**, 243 (2006).

[28] N. Li, A. Wang, Z. Liu, X. Wang, M. Zheng, Y. Huang, T. Zhang, *Appl. Catal. B-Environ.* **62**, 292 (2006).

[29] N. Essayem, V. Martin, A. Riondel, A.J.C. Vedrine, *Appl. Catal. A-Gen.* **326**, 74 (2007).

[30] Y. Suchorski, J. Gottfriedsen, R. Wrobel, B. Strzelczyk, H. Weiss, *Solid State Phenom.* **128**, 115 (2007).

[31] Y. Suchorski, L. Rihko-Struckmann, F. Klose, Y. Ye, M. Alandjiyska, K. Sundmacher, H. Weiss, *Appl. Surf. Sci.* **249**, 231 (2005).

[32] http://www.casaxps.com.

[33] R. Garvie, *J. Phys. Chem.* **69**, 1238 (1965).

[34] S. Lütkenhof, M. Neumann, A. Slebarski, *Phys. Rev. B* **52**, 13808 (1995).

[35] H. Ogasawara, A. Kotani, R. Potze, G.A. Zawadzky, B.T. Thole, *Phys. Rev. B* **44**, 5465 (1991).

[36] D.D. Sarma, C.N.R. Rao, *J. Electron. Spectrosc.* **20**, 25 (1980).

[37] Y. Uwamino, Y. Ishizuka, H. Yamatera, *J. Electron. Spectrosc.* **34**, 69 (1984).

[38] B.M. Reddy, B. Chowdhury, I. Ganesh, *J. Phys. Chem. B* **102**, 10176 (1998).

[39] A.E. Hughes, B.A. Sexton, *J. Electron. Spectrosc.* **50**, 15 (1990).

[40] G.W. Coulston, E.A. Thompson, N. Herron, *J. Catal.* **163**, 122 (1996).

[41] R. Kaufmann, H. Klewe-Nebenius, H. Moers, G. Pfennig, H. Jenett, H.J. Ache, *Surf. Interface Anal.* **11**, 502 (1988).

[42] C. Morant, J.M. Sanz, L. Galan, L. Soriano, *Surf. Sci.* **218**, 331 (1989).

[43] M.P. Seah, W.A. Dench, *Surf. Interface Anal.* **1**, 2 (1979).

[44] C.S. Fadley, *Prog. Surf. Sci.* **16**, 275 (1984).

[45] A. Jablonski, *Surf. Sci.* **586**, 115 (2005).